Isotopic yields of spallation residues produced in ^{136}Xe-induced reactions on deuterium at 500A MeV

J. Alcántara-Núñez,[1] J. Benlliure,[1,*] C. Paradela,[1,†] C. Pérez-Loureiro,[1,‡] J. L. Rodríguez-Sánchez,[1] L. Audouin,[2] A. Boudard,[3] E. Casarejos,[1,§] T. Enqvist,[4,‖] F. Farget,[5] M. Fernández-Ordóñez,[1] A. Heinz,[6,¶] V. Henzl,[4,#] D. Henzlova,[4,#] A. Kelić-Heil,[4] A. Lafriaskh,[2] S. Leray,[3] P. Napolitani,[2] J. Pereira,[1,‡] M. V. Ricciardi,[4] C. Stéphan,[2] K.-H. Schmidt,[4] C. Schmitt,[5] L. Tassan-Got,[2] C. Villagrasa,[3] C. Volant,[3] and O. Yordanov[4,**]

[1]*Universidad de Santiago de Compostela, E-15782 Santiago de Compostela, Spain*

[2]*Institut de Physique Nucléaire d'Orsay, F-91406 Orsay, France*

[3]*IRFU, DSM-CEA, F-91191 Gif-sur-Yvette Cedex, France*

[4]*GSI Helmholtzzentrum für Schwerionenforschung GmbH, D-64291 Darmstadt, Germany*

[5]*Grand Accélérateur National d'Ions Lourds, F-14076 Caen, France*

[6]*A.W. Wright Nuclear Structure Laboratory, Yale University, New Haven, Connecticut 06511, USA*

(Received 27 May 2015; published 10 August 2015)

Residual fragment production in reactions induced by ^{136}Xe projectiles impinging on a liquid deuterium target at 500A MeV has been measured at GSI. Projectile residues were unambiguously identified in atomic and mass numbers using the Fragment Separator as high-resolution zero-degree spectrometer. The isotopic production yields of these residuals were used to benchmark reference model calculations describing spallation reactions. In particular the energy dissipated in these reactions was assessed by comparing the production yields measured in this work with the ones obtained in reactions induced by ^{136}Xe projectiles on protons at 1000A and 500A MeV.

DOI: 10.1103/PhysRevC.92.024607 PACS number(s): 25.40.Sc, 24.10.Lx, 25.70.−z

I. INTRODUCTION

Spallation reactions are used in a broad range of research fields and applications [1]. Cosmic ray physics [2], radioactive beam factories [3], spallation neutron sources [4], and accelerator-driven subcritical power plants (ADS) [5,6] are some examples. All these applications require an accurate description of the light particles emitted, e.g., neutrons, or the residual nuclei produced. This interest justifies the effort to improve our knowledge of this reaction mechanism, from both an experimental and a theoretical viewpoint. Up to now, several experiments have been performed to characterize neutron and charged-particle emission in spallation reactions, as well as the yields of the residual nuclei (e.g., see [7] and references therein).

Spallation reactions are described as a two-step process. The fast interaction between hadrons and nuclei is generally modeled using intranuclear cascade codes. These semiclassical models have evolved from the rather simple approaches by Metropolis [8] and Bertini [9] to the most advanced versions of the ISABEL [10] and INCL [11] codes. The deexcitation of the highly excited remnants produced in the intranuclear cascade phase by emission of nucleons, clusters, gamma rays, or eventually by fission, is described by statistical codes based on the Weisskopf [12] or Hauser-Fesbach [13] formalisms. Among others, two of the most widely used deexcitation codes are ABLA [14] and GEMINI [15].

Precise knowledge of the isotopic yields of residual nuclei produced in spallation reactions is of utmost importance for the determination of the beam intensities that can be delivered by radioactive beam factories [16] or for the radiological characterization of the target assemblies used in spallation neutron sources or ADS [17]. Those production yields were determined in direct kinematics, bombarding heavy targets mostly with relativistic protons [18]. In this case the reaction residues do not leave the target material and can only be identified using gamma spectroscopic techniques. The main limitation of this technique is that it is not applicable to stable residues, and for unstable ones the measurement is done after β decay and consequently only isobaric identification is possible. To overcome this limitation inverse kinematic measurements were proposed. This technique allows for the unambiguous identification of each reaction remnant when high-resolution spectrometers are used [19].

The isotopic yields of residual fragments produced in spallation reactions have been investigated at GSI (Darmstadt) for a broad range of heavy systems, using the inverse kinematic technique. In particular, complete isotopic distributions of the residual nuclei produced in reactions induced by beams of ^{238}U [20,21], ^{208}Pb [22–25], and ^{197}Au [26,27] impinging on a cryogenic target filled with liquid hydrogen or deuterium at energies between 500A and 1000A MeV were measured. Because fission has a relevant role in these heavy systems, dedicated experiments where both fission fragments could

*Corresponding author: j.benlliure@usc.es

†Present address: EC-JRC, Institute for Reference Materials and Measurements, Retieseweg 111, B-2440 Geel, Belgium.

‡Present address: NSCL, East Lansing, MI 48824, USA.

§Present address: Universidade de Vigo, E-36310 Vigo, Spain.

‖Present address: Oulu Southern Institute and Department of Physics, University of Oulu, Oulu Finland.

¶Present address: Chalmers University of Technology, SE-412 96 Gothenburg, Sweden.

#Present address: Los Alamos National Laboratory, Los Alamos, NM, USA.

**Present address: INRNE, 72 Tzarigradsko Chaussee, BG-1784 Sofia, Bulgaria.

be measured in coincidence were performed with beams of ^{238}U [28], ^{208}Pb [29], and ^{181}Ta [30].

Lighter systems such as ^{136}Xe on hydrogen at 1000A [31], 500A [32], and 200A MeV [33] or ^{56}Fe at energies between 1500A and 300A MeV [34] have also been studied. These systems were investigated because they are of interest in cosmic-ray astrophysics but also to assess the radiation damages in structural materials used in spallation sources. Another argument justifying the interest in these systems is the very low contribution of fission, facilitating the benchmarking of intranuclear cascade models. According to this, the measurements of the reactions induced by ^{136}Xe projectiles on hydrogen at 200A, 500A, and 1000A MeV are contributing to validate the energy dissipation in spallation reactions.

In this work we propose another alternative to benchmark intranuclear cascade models based on the reaction of ^{136}Xe on deuterium at 500A MeV. The comparison of this reaction with results previously obtained with the same projectile impinging on protons at 500A [32] and 1000A MeV [31] is expected to provide additional constraints to reaction models. We expect that the most peripheral reactions with deuterium behave as the ones with protons at 500A MeV. However, more violent collisions with deuterium at 500A MeV should be closer to the reactions with protons at 1000A MeV.

The paper is organized as follows. In the next section we briefly present the experiment and the data reduction process. Then we discuss the measured cross sections in comparison to the results obtained with a hydrogen target at 500A and 1000A MeV. Finally we benchmark state-of-the-art intranuclear cascade models with the three sets of data.

II. THE EXPERIMENT

The experiment was performed at the GSI (Darmstadt) accelerator facilities providing a beam of ^{136}Xe at 500A MeV with an intensity varying between 10^5 and 10^8 ions per second. The beam had a pulsed structure with a complete cycle duration of 10 s and a spill length of 5 s. A secondary electron monitor SEETRAM [35] was used for the continuous monitoring of the beam intensity. The beam impinged onto a cryogenic target filled with liquid deuterium. The deuterium container was 1.1 cm thick (201 mg/cm^2) with entrance and exit windows made of titanium (33.6 mg/cm^2) and some additional layers of Mylar (8.3 mg/cm^2) for thermal isolation. Reaction products, emitted forward because of the kinematics, were analyzed using the Fragment Separator (FRS) [36] as a zero-degree magnetic spectrometer. A complete description of the FRS, its detection equipment, and the data sorting procedure can be found in Ref. [37]; here we just present a summary.

A. Experimental setup

The FRS is a high resolution ($B\rho/\Delta B\rho \approx 1500$) magnetic spectrometer. The two symmetric sections with an intermediate dispersive image plane guarantee the achromaticity of the system (see Fig. 1). The acceptance of this device in longitudinal momentum is $\Delta p/p \approx \pm 1.5\%$ and in polar angle 15 mrad around the central trajectory.

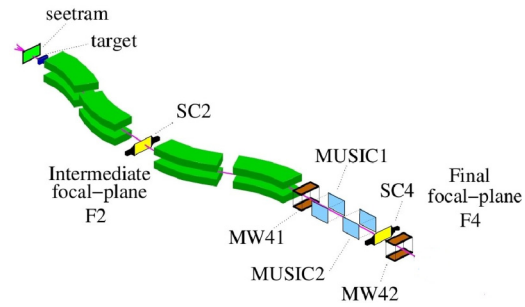

FIG. 1. (Color online) Schematic view of the Fragment Separator displaying only the dipole magnets and the detection equipment.

Nuclei traversing the FRS can be identified in mass over atomic number (A/Z), assuming they are fully stripped ($Z = q$), from the determination of their magnetic rigidity and velocity according to the following expression:

$$B\rho = \frac{m_o c}{e}\beta\gamma\frac{A}{q}, \tag{1}$$

where m_o is the nuclear mass unit, c the velocity of light, e the electron charge, and $\beta\gamma$ the relativistic velocity of the nuclei and the corresponding Lorentz factor. In the experiment the magnetic rigidity was determined from the transversal positions of the trajectories of each nucleus at the intermediate and final image planes, measured with two plastic scintillators (SC2 and SC4 in Fig. 1). These scintillators also provided the velocity from the time of flight of the nuclei between both detectors. Moreover, two multisampling ionization chambers (MUSIC1 and MUSIC2 in Fig. 1) located at the exit of the spectrometer provided the identification in atomic number of each nucleus from the measurement of the corresponding energy loss in the gas volume of the chamber.

B. Data evaluation

The unambiguous identification of the reaction products also requires a precise identification and separation of different atomic charge states. This separation can be achieved by combining the atomic number of each nucleus with the energy lost by that nucleus in the matter placed at the intermediate image plane of the spectrometer. This energy loss was obtained from the difference of the magnetic rigidity of the nuclei in the first and second parts of the spectrometer as explained in Ref. [38]. Any change in the atomic charge state of the nuclei when traversing the matter at the center of the spectrometer translates into a sizable change in the corresponding magnetic rigidity and then, in the energy loss, as shown in Fig. 2. In this figure we can clearly separate the contributions of nuclei fully stripped in the first section of the spectrometer but gaining an electron in the middle (group on the left), hydrogen-like nuclei in the first section that lose the electron (group on the right), and nuclei traversing the two sections of the FRS fulled stripped or as hydrogen-like nuclei (group in the middle).

In the present experiment the limited amount of matter at the intermediate image plane of the spectrometer did not allow us to separate fully stripped nuclei in both sections of the spectrometer from hydrogen-like ones. The probability of the latter

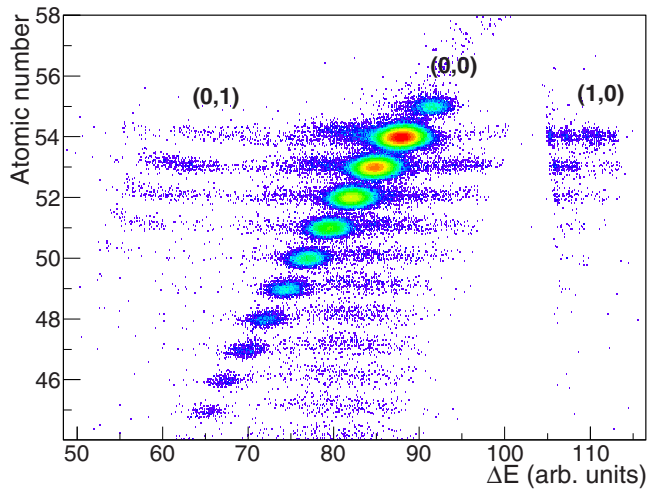

FIG. 2. (Color online) Cluster plot of the atomic number of the fragments transmitted in a setting of the FRS centered on ^{120}Cd as function of the energy lost by these fragments in the matter at the intermediate image plane of the spectrometer. The pairs of digits indicate the number of electrons carried by the respective nuclei in the first and second sections of the spectrometer.

is of the order of few per mil for the heavier nuclei investigated in this work and decreases very fast with the atomic number. However, for heavy neutron-rich nuclei this small probability can still result in a non-negligible contamination. For those nuclei, $A-3$ hydrogen-like fragments have an A/q similar to that of the fully stripped A isotopes. Because of the much larger cross sections of the $A-3$ fragments, between two and three orders of magnitude, the fraction of hydrogen-like ones would be comparable to the production of fully stripped A isotopes. Fortunately, at 500A MeV the resolving power of the FRS is sufficient to clearly separate in mass over atomic charge (A/q) the fully stripped A isotopes from the hydrogen-like $A-3$ fragments as explained in the following discussion of Fig. 3.

Figure 3 displays the identification matrix of the 685 nuclei measured in this experiment gating on the fully stripped condition (0,0) in Fig. 2. This figure was obtained overlapping the individual identification matrices obtained in 29 different magnetic settings of the FRS. These settings were centered on 16 isotopes of cadmium between ^{100}Cd and ^{127}Cd and 13 isotopes of arsenic between ^{67}As and ^{85}As. The figure illustrates the excellent resolution in atomic and mass number achieved in this measurement ($\Delta Z/Z \approx 6.1 \times 10^{-3}$ and $\Delta A/A \approx 1 \times 10^{-3}$). The calibration in atomic number was obtained from the largest production yields of xenon isotopes. We can also identify a vertical line in A/q corresponding to $N = Z$ nuclei providing thus the absolute calibration in mass number of all measured nuclei.

The figure shows the large range in elements and isotopes covered by this measurement. We identified the production of elements from barium down to argon, and for each of them long isotopic chains with a clear access to relatively neutron-rich nuclei for the heavier elements and neutron-deficient ones for the lighter elements. Residual nuclei of cesium and barium isotopes with one and two protons more than the xenon projectiles were produced in (n,p) charge-exchange reactions. In these reactions the elastic exchange of protons and neutrons between projectile and target nuclei, or the excitation of nucleon resonances with the subsequent emission of charged pions [39,40], may increase the number of protons in the residual nuclei.

In the top-right side of the figure we also identify the production of very neutron-rich residues. We observe the most neutron-rich nuclei that can be produced in nucleon removal processes, ^{135}I, ^{134}Te, ^{133}Sb, and ^{132}Sn, corresponding to the removal of up to four protons from ^{136}Xe. These reaction channels are relevant to investigate fluctuations in the excitation energy gained by the remnants in spallation reactions because in this case the excitation energy gained must be below the particle (neutron) evaporation threshold [41]. We also observe the production of even more neutron-rich nuclei, ^{136}Xe, ^{135}Te, and ^{134}Sb. These nuclei are produced in reactions combining proton removal and (p,n) charge-exchange processes as previously observed in Ref. [42]. In this region of very neutron-rich nuclei we can also identify contributions due to not fully stripped nuclei such as the one $(1e^-)$ and two $(2e^-)$ electron channels of the primary beam. We also observe $A-3$ hydrogen-like isotopes lying in between two full stripped nuclei, for example ^{132}I^{52+} in between fully stripped ^{135}I and ^{136}I.

III. MEASURED CROSS SECTIONS

The production cross sections of the different residual nuclei issued in the reaction investigated in this work were determined from the respective production yields, the flux of projectile nuclei, and the number of target atoms per surface unit. The flux of incoming projectiles was obtained by calibrating the current induced by the beam in the SEETRAM (Secondary Electron Transmission Monitor) in terms of particle number using a plastic scintillator as reference. The number of target atoms per surface unit was deduced from the target thickness. Due to the limited momentum acceptance of the FRS, the yield of many of the residual nuclei was determined by accounting for the fraction of transmitted nuclei in several consecutive magnetic tunings of the spectrometer as shown in Fig. 4. The yields measured with the empty target were subtracted from the deuterium-filled target yields to deduce the production yields in the deuterium only. The isobaric distribution of the measured yields of the residual nuclei produced with the filled and empty target are displayed in Fig. 5.

The yields of the residual nuclei obtained in reactions with deuterium were then corrected for the losses induced by the experimental setup. In particular, corrections due to the attenuation of beam particles in the target, losses of residual nuclei by secondary reactions in the target but also in the detectors placed at the intermediate image plane of the spectrometer, nonregistered events due to dead time of the data acquisition system, losses due to the limited angular transmission of the spectrometer or to incompletely stripped residual nuclei, and the efficiencies of the different detectors were taken into account.

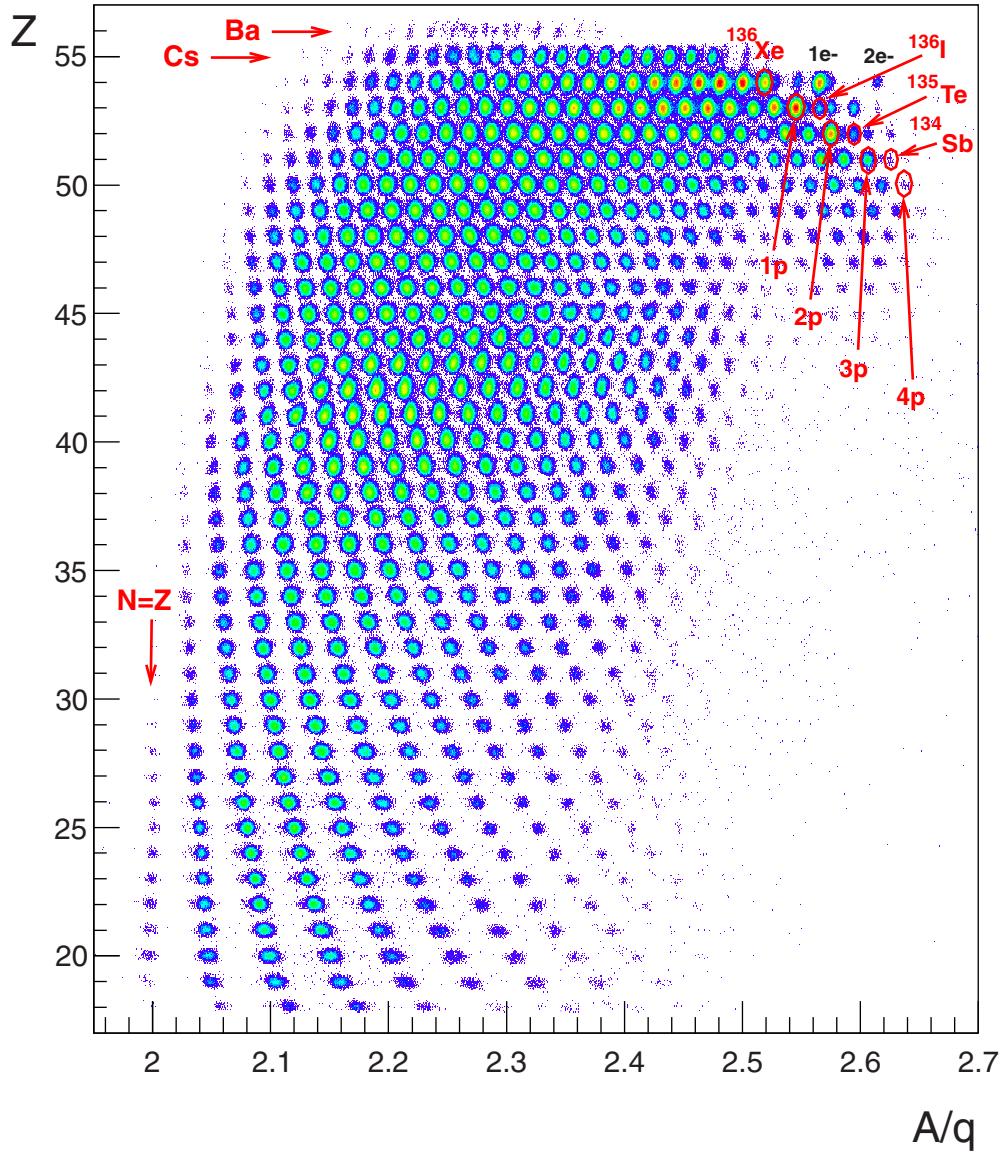

FIG. 3. (Color online) Cluster plot displaying the correlation between the atomic number (Z), determined from the energy loss measurements in the MUSIC detectors, and the mass-over-charge ratio (A/q) obtained from the magnetic rigidity and time-of-flight measurements for all the events registered in the 29 different magnetic tunings of the FRS used in this experiment. This plot provides the unambiguous identification in atomic and mass number of all the projectile residues produced in the reaction ^{136}Xe $+d$ at 500A MeV.

The corrections for the attenuation of the primary beam in the target and for secondary reactions of the residual fragments in the plastic scintillator located at the intermediate image plane were estimated from total reaction cross sections calculated with the code KAROL [43]. This correction amounted to less than 20% with an uncertainty of the order of 5%. Multiple reactions of the residual fragments in the target cause the depopulation of heavy neutron-rich fragments contaminating lighter neutron-deficient ones. This correction was implemented following the algorithm described in Ref. [31]. The dead time of the data acquisition system was kept below 30% and registered with a negligible uncertainty. The efficiency of the detectors was determined by crosschecking measurements between different detectors and was always above 95% with an uncertainty of a few percent. The probability of different charge states was evaluated with the code global [44]. The fraction of fully stripped ions for the heaviest elements measured in this experiment was around 95% with an uncertainty of 5%.

The angular transmission was the most relevant correction, in particular for the lighter residual fragments. This correction was obtained following the procedure described in Ref. [45]. The results are shown in Fig. 6 (solid line) in comparison to the same corrections for the reaction ^{136}Xe $+p$ at 1000A MeV reported in Ref. [31]. As shown in the figure, the limited aperture of the FRS ($\approx$15 mrad) reduces the angular transmission of the lightest nuclei, $A \approx 60$, to 30% while at 1000A MeV the transmission for the same nuclei amounts to 70%. This correction was estimated with an accuracy around 5%. In the inset of Fig. 6 we represent in a scatter plot the correlation

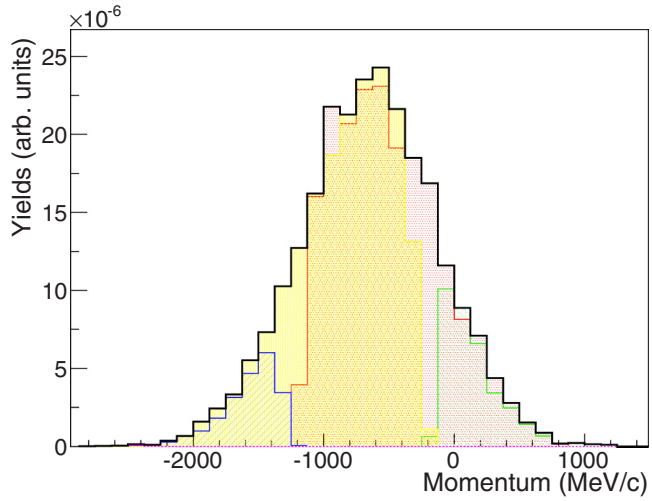

FIG. 4. (Color online) Longitudinal momentum in the frame defined by the projectile in the center of the target, for the nucleus ^{99}Rh, produced in the reaction ^{136}Xe(500A MeV) + d. The different areas correspond to the momentum intervals measured in different FRS magnetic settings.

between the mass number of the reaction residues and its polar angle for the reaction ^{136}Xe +d at 500A MeV as simulated with the intranuclear cascade code INCL4.6 [11] coupled to the deexcitation code ABLA07 [14]. The horizontal dashed line represents the maximum angular aperture of the FRS.

Following this procedure we determined the production cross sections of 530 residual nuclei issued from the reaction ^{136}Xe +d at 500A MeV. All these cross sections are shown in Fig. 7 on top of a chart of nuclides and listed in Table I. This figure nicely indicates the location of these residual

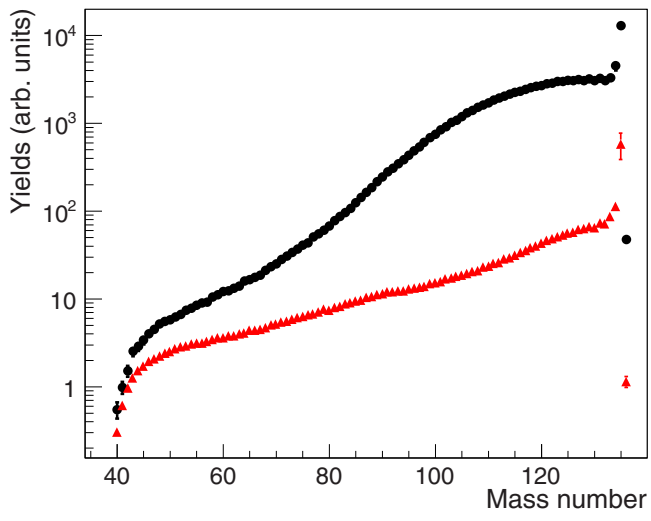

FIG. 5. (Color online) Isobaric production yields measured with the target filled with liquid deuterium (points) and those measured in the titanium windows with the empty target (triangles). The observed dramatic reduction in the production yields of the heaviest residual nuclei is explained by the small probability of the charge exchange processes leading to their formation.

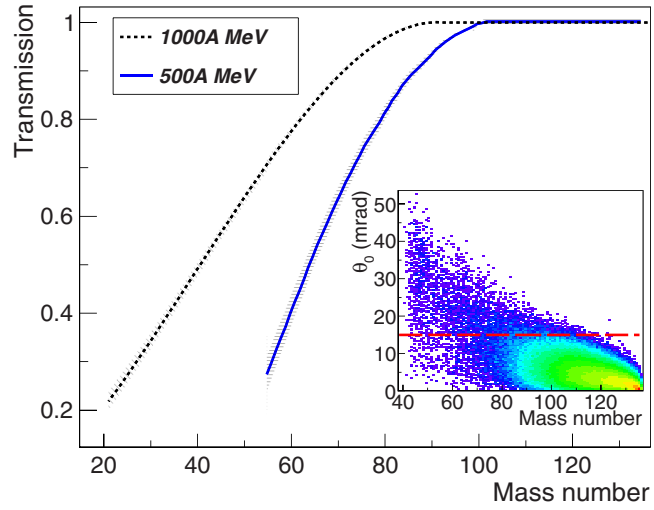

FIG. 6. (Color online) Angular transmission as a function of the mass number of the final residual nuclei evaluated according to Ref. [45] for the reactions ^{136}Xe +d at 500A MeV (solid line) and ^{136}Xe +p at 1000A MeV (dashed line). The inset represents a cluster plot of the simulated correlation between the mass number of the final fragments and its polar angle for the reaction ^{136}Xe +d at 500A MeV. The dashed line indicates the maximum angular aperture of the FRS.

nuclei in the chart of nuclides and the evolution of the production cross sections. As expected, the most abundant fragments are located close to the projectile nucleus, while the production decreases with decreasing mass number of the final residue. Concerning the isotopic composition, the most abundant nuclei have a neutron excess similar to the one of ^{136}Xe. The maximum of the production per element moves then towards more neutron-deficient isotopes in a tendency to reach the so-called "evaporation corridor" [46] at the left of the β-stability valley. For a given element we also see clearly how the production decreases for the most neutron-rich and neutron-deficient isotopes.

In Figs. 8 and 9 we display the isotopic distributions of the different elements produced in the investigated reaction.

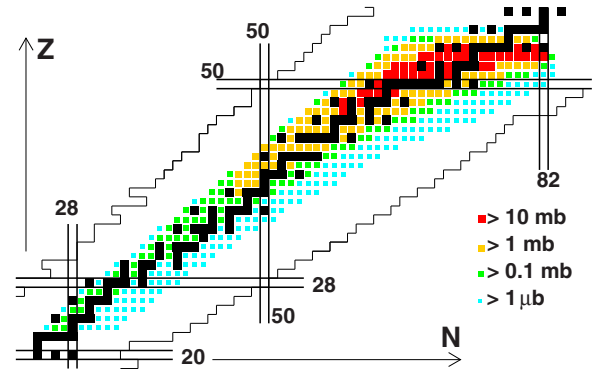

FIG. 7. (Color online) Residual nuclei produced in the reaction ^{136}Xe + deuterium at 500A MeV per nucleon identified in this work represented on top of a chart of nuclide. The color scale represents the production cross section, the black squares correspond to stable isotopes, and the lines indicate the limit of the known nuclides.

TABLE I. Isotopic cross sections of the residual nuclei produced in the reaction ^{136}Xe(500A MeV) + d together with their total associated uncertainties (statistical and systematical) indicated in parentheses.

Z	A	σ (mb)	Z	A	σ (mb)	Z	A	σ (mb)
23	48	0.074(0.002)	23	49	0.240(0.008)	23	50	0.204(0.007)
23	51	0.093(0.008)	23	52	0.050(0.005)	23	53	0.028(0.004)
23	54	0.007(0.002)	23	55	0.0011(0.0002)	23	56	0.00033(0.00006)
24	50	0.063(0.003)	24	51	0.184(0.009)	24	52	0.178(0.009)
24	53	0.119(0.009)	24	54	0.070(0.007)	24	55	0.022(0.004)
24	56	0.009(0.002)	24	57	0.003(0.001)	24	58	0.0014(0.0005)
25	52	0.039(0.002)	25	53	0.150(0.009)	25	54	0.177(0.013)
25	55	0.152(0.013)	25	56	0.074(0.007)	25	57	0.033(0.006)
25	58	0.015(0.003)	25	59	0.004(0.001)	25	60	0.002(0.001)
25	61	0.00047(0.00021)	26	54	0.028(0.002)	26	55	0.119(0.008)
26	56	0.196(0.011)	26	57	0.124(0.011)	26	58	0.094(0.009)
26	59	0.040(0.006)	26	60	0.020(0.004)	26	61	0.006(0.002)
26	62	0.004(0.001)	26	63	0.00042(0.00020)	27	56	0.004(0.001)
27	57	0.103(0.009)	27	58	0.188(0.014)	27	59	0.182(0.014)
27	60	0.109(0.011)	27	61	0.074(0.009)	27	62	0.0256(0.005)
27	63	0.010(0.003)	27	64	0.0034(0.0011)	27	65	0.0014(0.0006)
28	59	0.073(0.005)	28	60	0.195(0.015)	28	61	0.177(0.017)
28	62	0.148(0.014)	28	63	0.077(0.009)	28	64	0.040(0.007)
28	65	0.018(0.004)	28	66	0.004(0.002)	28	67	0.002(0.001)
28	68	0.00068(0.00036)	29	61	0.033(0.003)	29	62	0.131(0.013)
29	63	0.187(0.018)	29	64	0.159(0.015)	29	65	0.107(0.012)
29	66	0.057(0.009)	29	67	0.030(0.006)	29	68	0.012(0.003)
29	69	0.0048(0.0017)	29	70	0.0017(0.0008)	30	63	0.024(0.002)
30	64	0.155(0.016)	30	65	0.207(0.020)	30	66	0.202(0.019)
30	67	0.123(0.014)	30	68	0.078(0.011)	30	69	0.043(0.008)
30	70	0.017(0.004)	30	71	0.0063(0.0025)	30	72	0.0027(0.0011)
30	73	0.0006(0.0003)	31	66	0.088(0.010)	31	67	0.201(0.021)
31	68	0.229(0.023)	31	69	0.185(0.021)	31	70	0.111(0.015)
31	71	0.066(0.011)	31	72	0.035(0.007)	31	73	0.013(0.003)
31	74	0.005(0.002)	31	75	0.0016(0.0008)	32	68	0.090(0.010)
32	69	0.244(0.026)	32	70	0.297(0.030)	32	71	0.250(0.025)
32	72	0.193(0.023)	32	73	0.099(0.014)	32	74	0.054(0.010)
32	75	0.022(0.005)	32	76	0.010(0.003)	32	77	0.0026(0.0010)
32	78	0.00038(0.00051)	33	70	0.076(0.011)	33	71	0.246(0.026)
33	72	0.372(0.037)	33	73	0.370(0.037)	33	74	0.238(0.027)
33	75	0.165(0.021)	33	76	0.076(0.013)	33	77	0.048(0.008)
33	78	0.016(0.004)	33	79	0.0071(0.0021)	33	80	0.0020(0.0010)
34	72	0.025(0.004)	34	73	0.258(0.030)	34	74	0.452(0.044)
34	75	0.446(0.042)	34	76	0.343(0.036)	34	77	0.225(0.027)
34	78	0.137(0.019)	34	79	0.069(0.011)	34	80	0.029(0.006)
34	81	0.011(0.003)	34	82	0.005(0.002)	34	83	0.0010(0.0007)
35	75	0.210(0.025)	35	76	0.439(0.047)	35	77	0.553(0.054)
35	78	0.432(0.044)	35	79	0.348(0.038)	35	80	0.215(0.026)
35	81	0.125(0.017)	35	82	0.057(0.009)	35	83	0.025(0.006)
35	84	0.007(0.003)	35	85	0.0022(0.0012)	35	86	0.0009(0.0007)
36	77	0.159(0.019)	36	78	0.515(0.053)	36	79	0.606(0.058)
36	80	0.655(0.063)	36	81	0.487(0.051)	36	82	0.327(0.039)
36	83	0.200(0.027)	36	84	0.099(0.014)	36	85	0.040(0.009)
36	86	0.015(0.005)	36	87	0.0052(0.0018)	36	88	0.0013(0.0009)
37	79	0.017(0.002)	37	80	0.381(0.044)	37	81	0.780(0.075)
37	82	0.810(0.077)	37	83	0.717(0.071)	37	84	0.502(0.056)
37	85	0.327(0.040)	37	86	0.170(0.024)	37	87	0.067(0.0136)
37	88	0.027(0.0102)	37	89	0.011(0.004)	37	90	0.003(0.001)
37	91	0.0009(0.0008)	38	82	0.428(0.048)	38	83	0.862(0.084)
38	84	1.08(0.10)	38	85	1.03(0.10)	38	86	0.802(0.084)
38	87	0.505(0.064)	38	88	0.263(0.039)	38	89	0.128(0.020)

TABLE I. (*Continued.*)

Z	A	σ (mb)	Z	A	σ (mb)	Z	A	σ (mb)
38	90	0.058(0.016)	38	91	0.025(0.014)	38	92	0.008(0.003)
38	93	0.0021(0.0015)	38	94	0.00051(0.00037)	39	84	0.254(0.030)
39	85	0.939(0.099)	39	86	1.42(0.14)	39	87	1.50(0.15)
39	88	1.17(0.13)	39	89	0.801(0.094)	39	90	0.454(0.078)
39	91	0.230(0.045)	39	92	0.103(0.031)	39	93	0.048(0.016)
39	94	0.024(0.016)	39	95	0.0070(0.0049)	39	96	0.0013(0.0009)
39	97	0.0004(0.0005)	40	86	0.164(0.022)	40	87	1.03(0.12)
40	88	1.84(0.20)	40	89	2.11(0.24)	40	90	1.74(0.19)
40	91	1.17(0.16)	40	92	0.734(0.120)	40	93	0.417(0.075)
40	94	0.202(0.033)	40	95	0.101(0.027)	40	96	0.048(0.023)
40	97	0.018(0.014)	40	98	0.0083(0.0059)	40	99	0.0021(0.0015)
41	89	1.07(0.11)	41	90	2.25(0.25)	41	91	2.76(0.32)
41	92	2.29(0.28)	41	93	1.82(0.23)	41	94	1.18(0.17)
41	95	0.757(0.118)	41	96	0.419(0.098)	41	97	0.219(0.054)
41	98	0.097(0.025)	41	99	0.047(0.023)	41	100	0.019(0.012)
41	101	0.007(0.005)	41	102	0.0013(0.0009)	42	91	1.11(0.12)
42	92	2.60(0.28)	42	93	3.18(0.35)	42	94	3.16(0.38)
42	95	2.57(0.32)	42	96	2.00(0.29)	42	97	1.30(0.21)
42	98	0.785(0.148)	42	99	0.422(0.094)	42	100	0.21(0.063)
42	101	0.091(0.032)	42	102	0.044(0.020)	42	103	0.017(0.009)
42	104	0.005(0.003)	42	105	0.0014(0.0012)	43	93	1.05(0.11)
43	94	2.62(0.28)	43	95	3.87(0.42)	43	96	4.07(0.46)
43	97	3.84(0.45)	43	98	3.03(0.37)	43	99	2.27(0.30)
43	100	1.31(0.20)	43	101	0.813(0.157)	43	102	0.415(0.111)
43	103	0.205(0.064)	43	104	0.083(0.033)	43	105	0.037(0.021)
43	106	0.015(0.009)	43	107	0.0046(0.0038)	43	108	0.0008(0.0005)
44	95	0.730(0.079)	44	96	2.66(0.27)	44	97	4.20(0.45)
44	98	5.25(0.57)	44	99	5.43(0.60)	44	100	4.72(0.54)
44	101	3.65(0.48)	44	102	2.34(0.34)	44	103	1.48(0.25)
44	104	0.804(0.162)	44	105	0.438(0.112)	44	106	0.197(0.067)
44	107	0.084(0.034)	44	108	0.031(0.013)	44	109	0.014(0.010)
44	110	0.005(0.004)	44	111	0.0006(0.0004)	44	112	0.00019(0.00016)
45	97	0.468(0.050)	45	98	2.29(0.24)	45	99	4.65(0.50)
45	100	6.08(0.68)	45	101	7.09(0.79)	45	102	6.44(0.74)
45	103	5.48(0.65)	45	104	3.86(0.49)	45	105	2.69(0.37)
45	106	1.63(0.26)	45	107	0.895(0.168)	45	108	0.426(0.105)
45	109	0.208(0.074)	45	110	0.087(0.043)	45	111	0.032(0.018)
45	112	0.014(0.009)	45	113	0.0034(0.0025)	45	114	0.00089(0.00081)
45	115	0.00020(0.00019)	45	116	$9.9\times10^{-5}(4.3\times10^{-5})$	46	99	0.087(0.009)
46	100	2.04(0.21)	46	101	4.49(0.48)	46	102	7.08(0.77)
46	103	8.60(0.94)	46	104	8.56(0.94)	46	105	7.72(0.87)
46	106	6.15(0.72)	46	107	4.42(0.54)	46	108	2.82(0.38)
46	109	1.67(0.25)	46	110	0.917(0.167)	46	111	0.462(0.118)
46	112	0.237(0.074)	46	113	0.103(0.041)	46	114	0.040(0.021)
46	115	0.014(0.012)	46	116	0.004(0.003)	46	117	0.0017(0.0012)
46	118	0.00059(0.00039)	46	119	0.00029(0.00015)	46	120	$9.9\times10^{-5}(8.9\times10^{-5})$
47	102	1.31(0.14)	47	103	4.14(0.43)	47	104	6.94(0.72)
47	105	9.46(0.97)	47	106	10.9(1.2)	47	107	10.2(1.1)
47	108	9.01(0.98)	47	109	7.01(0.79)	47	110	4.88(0.58)
47	111	3.27(0.42)	47	112	1.93(0.28)	47	113	1.11(0.19)
47	114	0.585(0.114)	47	115	0.282(0.068)	47	116	0.134(0.045)
47	117	0.068(0.029)	47	118	0.024(0.013)	47	119	0.013(0.006)
47	120	0.005(0.003)	47	121	0.0011(0.0005)	47	122	0.00049(0.00025)
47	123	0.00020(0.00012)	48	104	0.718(0.076)	48	105	3.27(0.34)
48	106	6.92(0.71)	48	107	10.3(1.0)	48	108	12.8(1.3)
48	109	13.0(1.4)	48	110	12.1(1.3)	48	111	10.1(1.1)
48	112	7.99(0.88)	48	113	5.30(0.62)	48	114	3.71(0.46)

TABLE I. (*Continued*.)

Z	A	σ (mb)	Z	A	σ (mb)	Z	A	σ (mb)
48	115	2.21(0.30)	48	116	1.31(0.20)	48	117	0.700(0.131)
48	118	0.392(0.084)	48	119	0.182(0.050)	48	120	0.097(0.036)
48	121	0.045(0.033)	48	122	0.017(0.007)	48	123	0.006(0.002)
48	124	0.0022(0.0006)	48	125	0.0009(0.0003)	48	126	$19.8\times10^{-5}(6.1\times10^{-5})$
49	106	0.095(0.011)	49	107	2.10(0.22)	49	108	5.46(0.56)
49	109	9.51(0.97)	49	110	12.9(1.3)	49	111	15.3(1.6)
49	112	15.2(1.6)	49	113	14.3(1.5)	49	114	12.1(1.3)
49	115	9.19(0.99)	49	116	6.67(0.74)	49	117	4.79(0.55)
49	118	2.94(0.37)	49	119	1.83(0.24)	49	120	1.06(0.15)
49	121	0.651(0.11)	49	122	0.341(0.069)	49	123	0.148(0.052)
49	124	0.065(0.020)	49	125	0.034(0.007)	49	126	0.012(0.004)
49	127	0.005(0.002)	49	128	0.0013(0.0003)	49	129	$29.7\times10^{-5}(6.6\times10^{-5})$
50	109	0.908(0.105)	50	110	3.74(0.41)	50	111	8.10(0.85)
50	112	12.6(1.3)	50	113	16.2(1.6)	50	114	17.8(1.8)
50	115	17.8(1.8)	50	116	16.7(1.7)	50	117	14.1(1.5)
50	118	11.8(1.3)	50	119	8.93(0.98)	50	120	6.25(0.71)
50	121	4.33(0.52)	50	122	2.88(0.35)	50	123	1.79(0.23)
50	124	1.11(0.15)	50	125	0.62(0.09)	50	126	0.308(0.121)
50	127	0.168(0.036)	50	128	0.075(0.017)	50	129	0.022(0.004)
50	130	0.0065(0.0011)	50	131	0.0011(0.0003)	50	132	$9.9\times10^{-5}(3.2\times10^{-5})$
51	111	0.014(0.002)	51	112	1.67(0.21)	51	113	4.97(0.57)
51	114	9.27(1.00)	51	115	14.2(1.5)	51	116	16.9(1.8)
51	117	19.8(2.0)	51	118	20.4(2.1)	51	119	19.4(2.0)
51	120	17.4(1.8)	51	121	15.3(1.6)	51	122	12.5(1.3)
51	123	9.96(1.1)	51	124	7.51(0.80)	51	125	5.46(0.59)
51	126	3.71(0.43)	51	127	2.57(0.32)	51	128	1.67(0.54)
51	129	0.889(0.242)	51	130	0.503(0.064)	51	131	0.180(0.026)
51	132	0.047(0.005)	51	133	0.008(0.001)	51	134	$9.9\times10^{-5}(2.9\times10^{-5})$
52	114	0.642(0.088)	52	115	2.60(0.32)	52	116	6.20(0.69)
52	117	10.0(1.1)	52	118	14.5(1.5)	52	119	18.4(1.9)
52	120	21.1(2.1)	52	121	23.3(2.4)	52	122	23.6(2.4)
52	123	23.4(2.4)	52	124	21.6(2.2)	52	125	18.9(1.9)
52	126	16.7(1.7)	52	127	13.8(1.4)	52	128	11.8(1.2)
52	129	9.26(0.95)	52	130	6.99(1.08)	52	131	5.03(1.33)
52	132	3.43(1.02)	52	133	1.86(0.47)	52	134	0.372(0.117)
52	135	0.0042(0.0008)	53	116	0.107(0.018)	53	117	1.01(0.15)
53	118	2.90(0.36)	53	119	6.01(0.68)	53	120	9.38(1.01)
53	121	13.9(1.4)	53	122	16.8(1.7)	53	123	21.6(2.2)
53	124	23.4(2.3)	53	125	27.5(2.7)	53	126	27.1(2.7)
53	127	29.7(2.9)	53	128	27.4(2.7)	53	129	29.8(2.9)
53	130	26.1(2.6)	53	131	28.1(2.7)	53	132	23.6(2.3)
53	133	26.0(5.8)	53	134	23.4(3.3)	53	135	28.1(3.4)
53	136	0.138(0.030)	54	118	0.062(0.017)	54	119	0.378(0.073)
54	120	1.17(0.20)	54	121	2.21(0.33)	54	122	4.34(0.56)
54	123	6.60(0.79)	54	124	9.53(1.07)	54	125	12.3(1.3)
54	126	15.8(1.7)	54	127	18.9(1.9)	54	128	22.0(2.2)
54	129	25.4(2.6)	54	130	28.1(2.8)	54	131	32.0(3.2)
54	132	34.3(3.3)	54	133	39.1(3.8)	54	134	54.0(5.2)
54	135	79.0(7.6)	55	119	0.0044(0.0049)	55	120	0.029(0.019)
55	121	0.080(0.035)	55	122	0.216(0.075)	55	123	0.497(0.135)
55	124	0.914(0.191)	55	125	1.34(0.25)	55	126	2.00(0.31)
55	127	2.63(0.39)	55	128	3.39(0.45)	55	129	4.17(0.53)
55	130	4.73(0.57)	55	131	5.33(0.63)	55	132	5.61(0.64)
55	133	5.55(0.62)	55	134	4.22(0.47)	55	135	2.61(0.30)
55	136	0.92(0.13)	56	123	0.004(0.006)	56	124	0.016(0.012)
56	125	0.024(0.018)	56	126	0.033(0.021)	56	127	0.036(0.022)
56	128	0.042(0.020)	56	129	0.039(0.022)	56	130	0.044(0.025)

TABLE I. (*Continued.*)

Z	A	σ (mb)	Z	A	σ (mb)	Z	A	σ (mb)
56	131	0.030(0.018)	56	132	0.013(0.008)	56	133	0.006(0.004)
56	134	0.0027(0.0016)	56	135	0.00099(0.00061)			

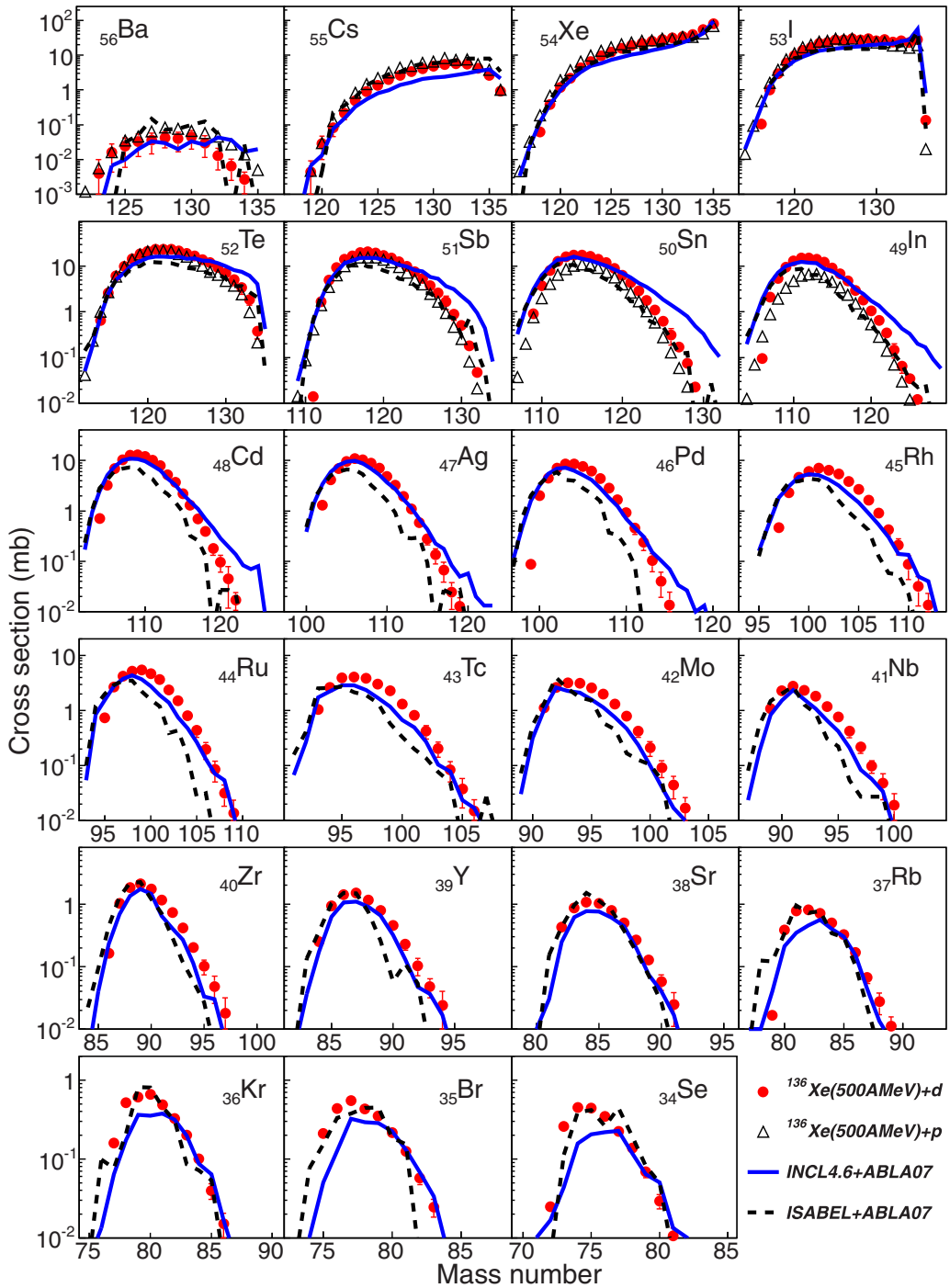

FIG. 8. (Color online) Isotopic distributions of the production cross sections of the projectile residues produced in the reaction ^{136}Xe $+d$ at 500A MeV corresponding to elements from barium to selenium. Open triangles represent cross sections obtained for the reaction ^{136}Xe $+p$ at 500A MeV from Ref. [32] and the lines represent different model calculations.

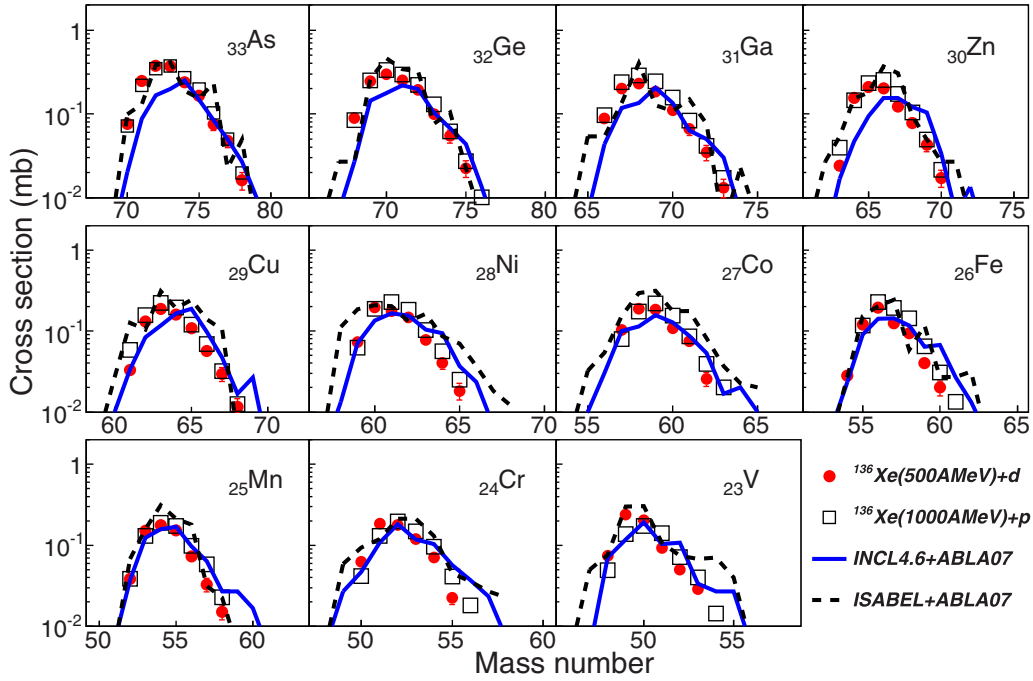

FIG. 9. (Color online) Isotopic distributions of the production cross sections of the projectile residues produced in the reaction ^{136}Xe $+d$ at 500A MeV corresponding to elements from arsenic to vanadium. Open squares represent cross sections obtained for the reaction ^{136}Xe $+p$ at 1000A MeV from Ref. [31] and the lines represent different model calculations.

We could determine the production cross sections of residual nuclei over long isotopic chains of elements from barium down to vanadium with very good accuracy. Indeed, the error bars were obtained combining statistic and systematic uncertainties. The statistical uncertainty was below a few per mil for most of the measured nuclei, and only for the most neutron-rich or neutron-deficient nuclei, with very small production cross sections, this uncertainty could be larger than 20%. Systematic uncertainties were obtained from the accuracy in the the target thickness, in the beam intensity, and in the different corrections that were applied to the measured yields. The quadratic sum of all these contributions amounted at most to 20%.

The shapes of the isotopic distributions shown in Figs. 8 and 9 are mostly determined by the deexcitation process of the prefragments produced in the interaction between ^{136}Xe and deuterium. Isotopes of xenon and indium are produced in very peripheral reactions where the ^{136}Xe projectiles lose at most one proton and/or a neutron, and the corresponding prefragment gains little excitation energy. These relatively neutron-rich prefragments deexcite mostly by evaporating neutrons leading to the observed asymmetric distribution of final residues. Isotopes of lighter elements are produced in more violent collisions where the projectile nucleus loses several protons and neutrons and the prefragments with a neutron excess similar to that of the the projectile nuclei are produced with high excitation energies. Under such conditions the prefragments deexcite by evaporating mostly neutrons but also protons. This evaporation process explains why the mean neutron excess of the final fragments is reduced approaching the situation for which the energy cost for the evaporation of protons and neutrons becomes equal. For lighter elements this tendency changes and the average neutron excess moves gradually away from the neutron-deficient side as discussed in Ref. [31].

IV. RESULTS AND DISCUSSION

A. Comparison with similar reactions

The comparison of the cross sections measured in this work with the ones previously obtained for the reactions ^{136}Xe $+p$ at 1000A MeV [31] and at 500A MeV [32] can help us to assess the energy dissipated in spallation reactions. Such a comparison is shown in Figs. 8–10. In Fig. 8 we compare the isotopic distributions measured in this work (points) with the ones obtained for the reaction ^{136}Xe $+p$ at 500A MeV for elements from barium to indium (open triangles), while in Fig. 9 we compare our results with the ones measured for the reaction ^{136}Xe $+p$ at 1000A MeV for elements from arsenic to vanadium (open squares). This comparison shows a very good agreement between the production cross sections of the heaviest fragments, barium to tellurium, obtained in the reactions induced by ^{136}Xe on protons and deuterons at 500A MeV. For lighter elements, the production cross sections obtained with the hydrogen target are smaller than the ones measured with the deuterium target. The production cross sections of the lightest elements shown in Fig. 9 also show a good agreement for the reactions induced on deuterons at 500A MeV and on protons at 1000A MeV.

This agreement between these reactions in different ranges of mass of the final residual nuclei can also be observed in the isobaric distributions of the measured cross sections

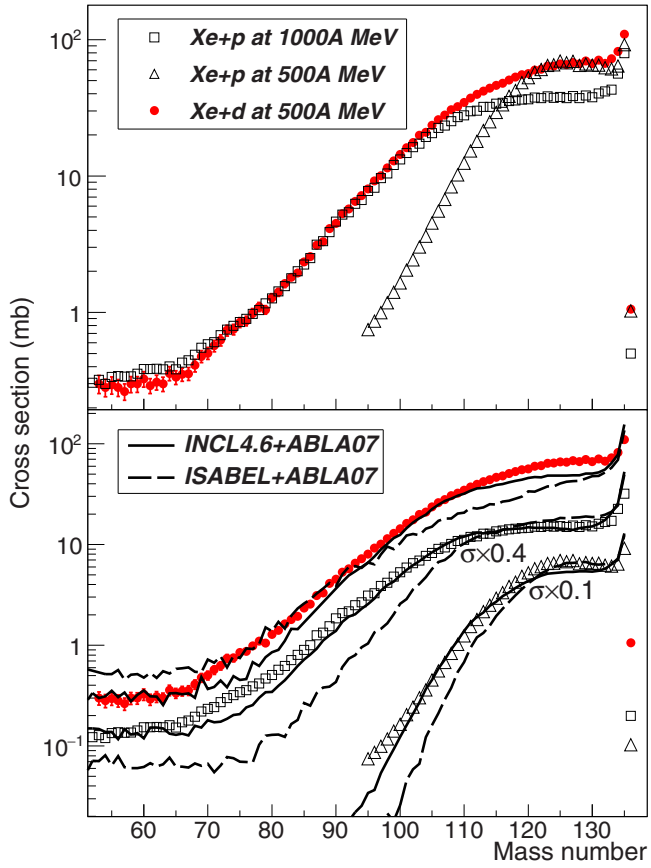

FIG. 10. (Color online) Isobaric distribution of the production cross sections of the residual nuclei measured in the reaction ^{136}Xe $+d$ at 1000A MeV (points) compared to the results previously obtained for the reactions ^{136}Xe $+p$ at 500A MeV (open triangles) and ^{136}Xe $+p$ at 1000A MeV (open squares). In the lower panel the data are compared to predictions obtained with the codes INCL and ISABEL. The important reduction in the production yields of the heaviest residual nuclei is explained by the small probability of the charge exchange processes leading to their formation.

displayed in the upper panel of Fig. 10. The figure shows a good agreement of the cross sections obtained with protons and deuterons at 500A MeV for the heaviest residues ($A > 120$). The same agreement is found for the reactions induced by ^{136}Xe on deuterons at 500A MeV and protons at 1000A MeV for the lightest residues ($A < 100$).

These results can be explained if one considers that the heaviest fragments are produced in very peripheral collisions where only one of the two nucleons from deuterium impinges on ^{136}Xe projectiles. In that scenario the main difference between the two targets, hydrogen and deuterium, is the possibility for the deuteron to also involve entrance channels where the interacting nucleon is a neutron. Those collisions are affected by the slightly different cross sections of the proton-proton and neutron-neutron primary collisions, but also by the formation of prefragments with a slightly different excess of protons or neutrons.

The comparison shown in Fig. 8 indicates that the production cross sections measured with protons and deuterons for elements from cesium down to tellurium look very similar. A closer inspection reveals that the production of barium and cesium isotopes is slightly larger with the proton target, while the most neutron-rich isotopes of xenon, indium, and tellurium present slightly larger production cross sections for the deuterium target. These small differences could be explained by the role of charge-exchange reactions, in particular the elastic ones dominating in the energy range covered by this experiment. Elastic (n,p) collisions in the projectile nuclei leading to the production of cesium and barium require a (p,n) reaction in the target. In that picture, only the proton in the deuteron should contribute to the production of these residual nuclei, and one would expect identical productions with the proton and deuteron targets. The observed deviations could indicate that neutrons in deuterons also contribute, exciting the charge exchange remnants, and therefore reducing their survival probability. The enhancement of the production of neutron-rich isotopes in heavy residues can be explained by (p,n) reactions in the projectiles that are only possible in collisions with target neutrons.

For elements lighter than tellurium, the larger cross sections obtained with the deuterium target indicate that both nucleons from the target interact with the projectile nuclei. In that case, the excitation energy gained by the projectile prefragments is larger, resulting in longer deexcitation chains, which enhances the population of lighter residual nuclei. This effect is clearly seen in the isobaric distributions shown in the upper panel of Fig. 10.

Below mass number 100, the isobaric distributions of the production cross sections of residual nuclei coincide for reactions induced by ^{136}Xe projectiles impinging on protons at 1000A MeV and on deuterons at 500A MeV, as shown in the upper panel of Fig. 10. The same conclusion is obtained from Fig. 9 showing coincident results for the isotopic production cross sections of the lightest residual nuclei produced in these two reactions. The data comparison of 500 MeV deuterons and 1000 MeV protons reveals similar energy dissipation in the two systems for the most central collisions.

This conclusion suggests that the description of these reactions in terms of a sequence of nucleon-nucleon collisions (impulse approximation), followed by intranuclear cascade models, is efficient in describing the excitation-energy distribution of the hot residues. On the other hand, the difference in the isobaric distributions obtained for reactions induced by ^{136}Xe projectiles on protons at 500A MeV and at 1000A MeV or deuterons at 500A MeV indicates that this observable is sensitive to the distribution of excitation energy gained by the prefragments during the first stage of the collision. This conclusion is also supported by the fact that in the range of masses greater than about half the mass of the system, the dominating process is compound nucleus decay where a clear correlation between the initial excitation energy and the mass of the final residue is expected.

These three reactions can also be compared in terms of the average neutron excess of the isotopic distributions $\langle N \rangle / Z$ depicted in Fig. 11 as a function of the atomic number of the final residual nuclei. The similar behavior observed for the different target nuclei and energies suggests a rather universal

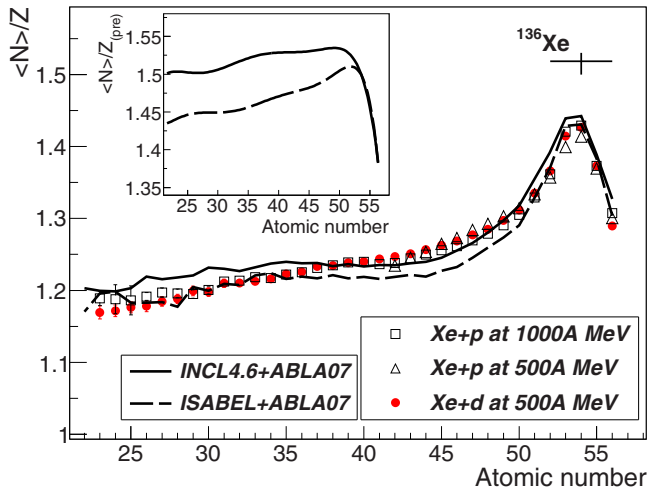

FIG. 11. (Color online) Average neutron excess of the isotopic distributions of the production cross sections of the residual nuclei measured in the reaction ^{136}Xe $+d$ at 1000A MeV (points), ^{136}Xe $+p$ at 500A MeV (open triangles), and ^{136}Xe $+p$ at 1000A MeV (open squares) as a function of the atomic number of the final residual nuclei. The data are compared with predictions obtained with the codes INCL and ISABEL. The inset shows the predicted neutron excess of the cascade prefragments obtained with the same model calculations.

pattern where the larger excitation energies for larger proton energies or heavier target nuclei do not affect the evolution of the average neutron excess of the residual nuclei but do modify their final masses.

The strong reduction of the average $\langle N\rangle/Z$ in residual nuclei close in atomic number to ^{136}Xe is explained by the relatively large neutron excess and moderate excitation energy of the initial prefragments. Under such conditions prefragments deexcite mainly by neutron evaporation. The production of lighter elements is characterized by prefragments with higher excitation energy where the deexcitation process opens other channels such as light-charged-particle emission. The competition between neutrons and light charged particles smooths the reduction of the neutron excess of the final fragments.

In Ref. [47] the final neutron excess of the residual nuclei observed in the reaction ^{136}Xe $+p$ at 1000A MeV was explained in relation to the process of prefragment formation in the early stage of the reaction. Dynamical effects were advocated therefore to explain the properties of light fragments far below half the mass of the projectile. Residues above half the mass of the projectile were found, on the other hand, to be consistent with a compound nucleus decay. However, even for relatively heavy fragments, the sequential decay result truncated before reaching the residue corridor due to the emission of light fragments and complex particles; this process is expected to affect in the same way also the system ^{136}Xe $+d$ at 500A MeV.

B. Benchmark of intranuclear cascade models

According to the previous discussions, the combination of the evolution of the isobaric distribution of the production cross sections and the neutron excess of the final residual nuclei provides important constraints for reaction models describing both stages of the reaction, the intranuclear cascade and the deexcitation. The reaction mechanism was discussed on the basis of the experimental data of ^{136}Xe $+p$ at 1000A MeV in Ref. [31] and in Ref. [47]. In the present work we will confront the measured data with predictions obtained from two widely used reaction codes describing the intranuclear cascade, the Liege intranuclear-cascade model (INCL) [11] and ISABEL [10]. In the particular case of the INCL model all calculations presented here are based on the version 4.6.

These two reaction codes are based on the intranuclear cascade approach describing the nucleon-nucleus interaction as a sequence of binary nucleon-nucleon collisions within a given volume determined by the size of the target nucleus. Inelastic collisions generate pions that propagate and participate in the intranuclear cascade. Nucleon-nucleon collisions are subject to Pauli blocking and may lead to the preequilibrium emission of nucleons or light clusters.

The main differences between these two codes are the following. INCL considers nucleons as point-like particles while ISABEL uses a continuous medium or Fermi sea which is perturbed by the collisions. The description of the nuclear density distributions is also different in both codes. In INCL nuclear density distributions is described by a Saxon-Wood distribution while ISABEL uses a folded Yukawa density distribution approximated by 16 constant-density regions. As the cascade evolves, the Fermi sea in ISABEL is depleted and the nuclear density is readjusted to calculate the evolution of the excited nucleons. The stopping criterion is also different. In INCL the stopping time is determined self-consistenly following a universal parametrization according to the mass number of the target nucleus. In ISABEL the cascade stops when the energies of the cascade particles are below a specific cutoff energy given by the Coulomb barrier plus two times the binding energy.

In both codes, the total excitation energy and angular momentum gained during the intranuclear cascade are described in terms of individual particle-hole excitations. The remaining excitation energy at the end of the intranuclear cascade is distributed among all the nucleons, producing a thermalized prefragment. The deexcitation of those prefragments is usually described using models based on the statistical evaporation of nucleons, clusters, gamma rays, and eventually by fission. In this work we have coupled the two intranuclear-cascade models to the ABLA07 [39] deexcitation code.

The model predictions for the isotopic distributions of the final reaction residues are compared to the measured data in Figs. 8 and 9. A first analysis indicates that ISABEL (dotted line) is better at describing the isotopic distributions of the heaviest fragments, while for intermediate-mass fragments INCL (solid line) seems to be closer to the data. Finally, both codes provide a reasonable description of the lightest fragments shown in Fig. 9.

The INCL code has difficulties in describing the heaviest nuclei which are supposed to be produced in the most peripheral reactions governed by few nucleon-nucleon collisions. The most neutron-rich isotopes of xenon and

cesium are reasonably well described but the other cross sections in these isotopic chains are clearly under-predicted. The code also overpredicts the production of the most neutron-rich fragments and underestimates the production of the most produced isotopes between tellurium and cadmium.

It is not obvious how to find a single argument explaining all these effects. One could think that the underestimation of the cesium isotopes should be related to the charge-exchange process responsible for the production of these nuclei via (n,p) reactions in the projectile nucleus [39] while the overprediction of neutron-rich residues should be linked to (p,n) [42] or proton-removal channels [41]. In principle one could relate the observed deviations to the excitation energy gained in these processes. An excess of the excitation energy gained in the charge-exchange process would deplete the production of cesium isotopes as observed. However, the overproduction of the neutron-rich isotopes could only be explained by an underestimation of the excitation energy gained in (p,n) charge exchange or proton-removal processes. Because both consequences seem contradictory, another explanation is required.

The description of the proton and neutron densities at the periphery of ^{136}Xe could also be at the origin of the observed deficiencies in the model predictions. An overestimation of the proton density at the nuclear periphery would inhibit (n,p) reaction channels producing cesium fragments and would enhance (p,n) and proton-removal channels producing the most neutron-rich residues. A new version of the INCL code with a more realistic description of the radial density of protons and neutrons seems to point in that direction [48]. For intermediate and light residues INCL provides an overall satisfactory description of the isotopic distributions.

The ISABEL code provides a slightly better description of the most peripheral collisions. The isotopic distributions of cesium and barium fragments produced in projectile (n,p) collisions are rather well reproduced while no apparent overproduction for the most neutron-rich isotopes of indium and tellurium is observed. However, ISABEL clearly underpredicts the cross sections of the most produced isotopes from xenon to indium and the most neutron-rich ones between indium and zirconium. The isotopic distributions of lighter elements are rather well described. The fact that ISABEL reproduces rather well the cross sections of the residues produced in charge exchange and proton-removal processes may indicate that the reasons for the deficiencies in describing other residual nuclei are different to the ones discussed for the INCL code.

To discuss the energy dissipated in these reactions we use the isobaric distribution of the measured cross sections displayed in Fig. 10. In the lower panel of the figure we confront the two model calculations described above with the set of data used for this benchmarking. Considering that all these reactions are dominated by compound-nucleus decay, one expects a clear correlation between the isobaric distribution of the final fragments and the distribution of the excitation energy gained by the prefragments during the intranuclear cascade phase. This correlation is confirmed in the upper panel of the figure showing a broadening of the isobaric distribution with the initial total energy.

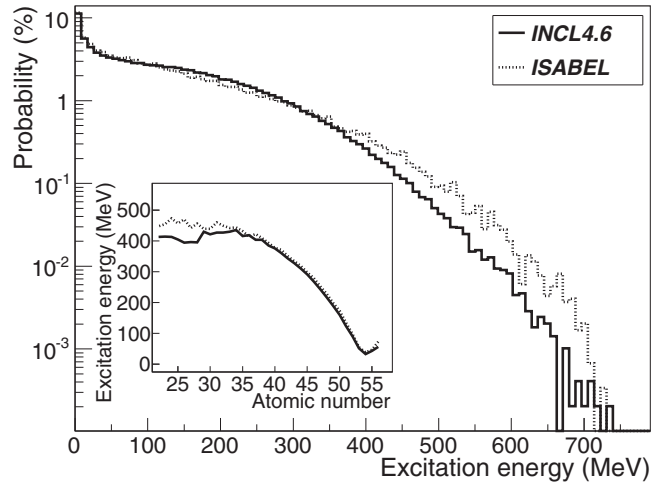

FIG. 12. Distribution of the excitation energy gained by the cascade prefragments as predicted by the INCL (solid line) and ISABEL (dotted line) codes. The inset represents the mean excitation energy as function of the atomic number of the final fragments obtained with the two codes.

For the three reactions under discussion the predictions obtained for the isobaric distributions of the residual nuclei with the code INCL follow a similar pattern. The code clearly underpredicts the cross sections of the heaviest masses and provides an overall reasonable description of the lightest fragments as mentioned earlier.

The results obtained with ISABEL are rather puzzling. For reactions induced by protons at 500A and 1000A MeV the code describes rather well the production of the heaviest residues while it clearly underestimates the light ones. In principle one could explain such a result by an underestimation of the excitation energy gained during the intranuclear cascade. However, the results obtained for the reaction induced by deuterons seem to follow the opposite pattern. In this case ISABEL underpredicts the isobar production of the heaviest fragments while it reproduces the lightest ones reasonably well.

The underestimation of the production cross sections of the heaviest residues produced in reactions with deuterium has a direct impact on the total reaction cross sections shown in Table II. Both codes underpredict the total reaction cross sections because the largest contribution originates from those residual nuclei. For the reactions induced by protons the situation is much better. Indeed, in the lower panel of Fig. 10 one observes a better description of the isobaric production cross sections of the heaviest residues. This analysis would indicate that part of the problem in the codes could be related to the description of the deuterium.

The differences in the predictions obtained with both codes could be related to the description of the energy dissipated in these collisions. However, the distributions of the excitation energy gained by the prefragments predicted with both codes are rather similar, as shown in Fig. 12. In particular, the low energy part of the distributions and the average excitation energy for the heavier residues, shown in the inset, are almost identical. Only for the lightest residues and the largest

TABLE II. Measured total reaction cross sections for the reactions induced by ^{136}Xe projectiles on deuterium at 500A MeV (this work), on protons at 1000A MeV (from Ref. [31]) and on protons at 500A MeV (from Ref. [32]) compared to the predictions obtained with the intranuclear cascade codes INCL and ISABEL coupled to the deexcitation code ABLA.

Reaction	Cross section (mb) Experiment	Cross section (mb) INCL4	Cross section (mb) ISABEL
^{136}Xe + d 500A MeV	1912 ± 133	1645	1358
^{136}Xe + p 1000A MeV	1393 ± 72	1378	1335
^{136}Xe + p 500A MeV	1388 ± 97	1265	1253

excitation energies are some differences between the two codes observed.

The other possible difference between the codes is in the predicted isotopic distributions of the cascade remnants. Figure 11 shows a clear difference in the average neutron excess of the final fragments predicted with both codes. For the heaviest residues both predictions are rather similar but as soon as we move away from the projectile atomic number we observe a systematic shift in the predicted neutron excess, the residues obtained with INCL being more neutron-rich. Unfortunately, none of the codes provides a good description of this observable for the full range of atomic numbers of the final residues. INCL describes the neutron excess of medium-mass residues and overestimates it for the lightest ones. In contrast, ISABEL underestimates the medium-mass residues and describes rather well the light ones.

The inset in Fig. 11 indicates that the predicted neutron excess of the prefragments produced during the cascade follows the same pattern observed for the final fragments after particle evaporation. Taking into account that we are using the same deexcitation code in both calculations with very similar distributions of the excitation energies of the prefragments, we can conclude that the difference in the final neutron excess of the fragments originates from the differences in the isotopic composition of the prefragments obtained with the two intranuclear cascade codes.

V. CONCLUSIONS

We have investigated the production of residual nuclei in reactions induced by ^{136}Xe projectiles at 500A MeV on a liquid deuterium target. The inverse kinematic allowed us to use a zero-degree high-resolution magnetic-spectrometer to unambiguously identify 530 residual nuclei in atomic and mass number, and determine their production cross sections with high accuracy.

The new data have been compared to previous measurements on the production of residual nuclei in reactions induced by ^{136}Xe projectiles at 500A and 1000A MeV on a liquid hydrogen target. The comparison of these three sets of data provides relevant information on the reaction mechanism. Heavy residual nuclei have almost identical production cross sections in reactions induced by ^{136}Xe projectiles at 500A MeV on hydrogen and deuterium. This result can be understood because those residual nuclei are produced in very peripheral collisions where only one of the nucleons in deuterium interacts with the projectile. We could then conclude that the interaction of ^{136}Xe nuclei with protons and neutrons at relativistic energies is identical with the exception of the charge-exchange reaction channels.

Light residual nuclei also present very similar production cross sections in reactions induced by ^{136}Xe projectiles at 500A MeV on deuterium and at 1000A MeV on hydrogen. In this case we concluded that in central collisions 1000A MeV protons and 500A MeV deuterons interact with the target nucleus in a very similar way. This finding validates the "impulse approximation" (sequence of independent two-particle collisions) used in intranuclear cascade models. On the other hand, the different production cross sections observed for heavy residues in these two reactions indicate that one cannot approximate the interaction of deuterons with nuclei by simply using protons with double energy, and an accurate description of the deuteron is necessary.

We have also used this set of data to benchmark two state-of-the-art intranuclear cascade codes, INCL and ISABEL. None of the codes provides a fully satisfactory description of all the data. INCL has difficulties to describe the production cross sections of residual nuclei close in atomic and mass number to ^{136}Xe produced in the most peripheral collisions. According to our analysis, this is probably due to an overprediction of the density of protons at the periphery of ^{136}Xe. However, INCL seems to describe the excitation energy dissipated in more central collisions rather well, providing a satisfactory description of the production cross sections of medium-mass and light residues.

ISABEL provides a very reasonable description of the heaviest residual nuclei produced in peripheral collisions with protons at 500A and 1000A MeV, but it seems to underpredict the excitation energy dissipated in the most violent collisions. Surprisingly, the code underpredicts the production of heavy residual nuclei in collisions with deuterium. The analysis of the total reaction cross sections suggests a problem with the description of the nucleon distribution in deuterons.

ACKNOWLEDGMENTS

This work was partially supported by the European Commission under the project ANDES-FP7-249671, the Spanish Ministerio de Ciencia e Innovación under projects FPA2010-22174-C02 and Consolider-CPAN-CSD2007-00042, and the Regional Government of Galicia under the program "Grupos de Referencia Competitiva 2013-011".

[1] D. Filges and F. Goldenbaum, *Handbook of Spallation Research* (Wiley-VCH, Weinheim, 2009).
[2] R. Schlickeiser, *Cosmic Ray Astrophysics* (Springer-Verlag, Berlin, 2002).
[3] P. Van Duppen, *Isotope Separation On Line and Post Acceleration*, The Euroschool Lectures on Physics with Exotic Beams, Vol. II (Springer-Verlag, Berlin, 2006).
[4] European Spallation Source, www.europeanspallationsource.se.
[5] C. D. Bowman, Nucl. Instrum. Methods A **320**, 336 (1992).
[6] F. Carminati *et al.*, CERN Technical Report No. CERN/AT/93-47 (unpublished).
[7] J. Benlliure, *Spallation Reactions in Applied and Fundamental Research*, The Euroschool Lectures on Physics with Exotic Beams, Vol. II (Springer-Verlag, Berlin, 2006).
[8] N. Metropolis *et al.*, Phys. Rev. **110**, 185 (1958).
[9] H. Bertini, Phys. Rev. **131**, 1801 (1963).
[10] Y. Yariv and Z. Fraenkel, Phys. Rev. C **24**, 488 (1981).
[11] A. Boudard, J. Cugnon, J.-C. David, S. Leray, and D. Mancusi, Phys. Rev. C **87**, 014606 (2013).
[12] V. F. Weisskopf and P. H. Ewing, Phys. Rev. **57**, 472 (1940).
[13] W. Hauser and H. Feshbach, Phys. Rev. **87**, 366 (1952).
[14] A. Kelić, M. V. Ricciardi, and K.-H. Schmidt, in *Joint ICTP-IAEA Advanced Workshop on Model Codes for Spallation Reactions*, IAEA INDC (NDS)-0530, edited by D. Filges *et al.* (IAEA Publications, Vienna, 2008), pp. 181–222.
[15] R. J. Charity *et al.*, Nucl. Phys. A **483**, 371 (1988).
[16] J. Benlliure, Eur. Phys. J. A **25**, 757 (2005).
[17] M. Medarde *et al.*, J. Nucl. Materials **411**, 72 (2011).
[18] I. Leya and R. Michel, Nucl. Instrum. Methods A **269**, 2487 (2011).
[19] P. Armbruster *et al.*, Phys. Rev. Lett. **93**, 212701 (2004).
[20] J. Taieb *et al.*, Nucl. Phys. A **724**, 413 (2003).
[21] M. Bernas *et al.*, Nucl. Phys. A **725**, 213 (2003).
[22] W. Wlazlo *et al.*, Phys. Rev. Lett. **84**, 5736 (2000).
[23] T. Enqvist *et al.*, Nucl. Phys. A **686**, 481 (2001).
[24] L. Audouin *et al.*, Nucl. Phys. A **768**, 1 (2006).
[25] B. Fernández-Domínguez *et al.*, Nucl. Phys. A **747**, 227 (2005).
[26] F. Rejmund *et al.*, Nucl. Phys. A **683**, 540 (2001).
[27] J. Benlliure *et al.*, Nucl. Phys. A **683**, 513 (2001).
[28] K.-H. Schmidt *et al.*, Phys. Rev. C **87**, 034601 (2013).
[29] J. L. Rodríguez-Sánchez *et al.*, Phys. Rev. C **90**, 064606 (2014).
[30] Y. Ayyad *et al.*, Phys. Rev. C **89**, 054610 (2014).
[31] P. Napolitani *et al.*, Phys. Rev. C **76**, 064609 (2007).
[32] L. Giot *et al.*, Nucl. Phys. A **899**, 116 (2013).
[33] C. Paradela *et al.* (unpublished).
[34] C. Villagrasa-Canton *et al.*, Phys. Rev. C **75**, 044603 (2007).
[35] A. R. Junghans *et al.*, Nucl. Instrum. Methods A **370**, 312 (1996).
[36] H. Geissel *et al.*, Nucl. Instrum. Methods B **70**, 286 (1992).
[37] J. Benlliure *et al.*, Phys. Rev. C **78**, 054605 (2008).
[38] E. Casarejos *et al.*, Phys. Rev. C **74**, 044612 (2006).
[39] A. Kelić *et al.*, Phys. Rev. C **70**, 064608 (2004).
[40] J. Vargas, J. Benlliure, and M. Caamaño, Nucl. Instrum. Methods A **707**, 16 (2013).
[41] J. Benlliure *et al.*, Nucl. Phys. A **660**, 87 (1999).
[42] A. I. Morales *et al.*, Phys. Rev. C **84**, 011601 (2011).
[43] P. J. Karol, Phys. Rev. C **11**, 1203 (1975).
[44] C. Scheidenberger *et al.*, Nucl. Instrum. Methods B **142**, 441 (1998).
[45] J. Benlliure *et al.*, Nucl. Instrum. Methods A **478**, 493 (2002).
[46] J. P. Dufour *et al.*, Nucl. Phys. A **387**, 157 (1982).
[47] P. Napolitani *et al.*, J. Phys. G: Nucl. Part. Phys. **38**, 115006 (2011).
[48] D. Mancusi, A. Boudard, J. Carbonell, J. Cugnon, J.-C. David, and S. Leray, Phys. Rev. C **91**, 034602 (2015).